*Korean J. of Chem. Eng.*, **8**(4), 220-226 (1991)

# AEROSOL ETCHING BY LOW-PRESSURE IMPACTION

**Sang-Moo Lee, Byung-Doo Chon and Sun-Geon Kim**

Department of Chemical Engineering, Chung Ang University, Seoul 156-756, Korea
*(Received 2 August 1991 • accepted 16 October 1991)*

**Abstract**—Low-pressure impaction technology has been applied to a new etch process using aerosol, called aerosol jet etching (AJE). Fine droplets (0.1 to 0.3 μm) produced by spray-evaporation-condensation method impinge on a substrate in low-pressure impactor and etches its surface. Investigations were carried out on the control of etchant droplet size, the critical diameter for impaction and the performance of AJE on patterned etching. The patterned etching on $SiO_2$ film reveals some advantages over conventional wet etching: the economic use of etchant, the reduction of waste disposal and the increase in controllability of etching. To make maximum use of the advantage of AJE, techniques of further decreasing the droplet size and depositing this small droplets on substrates need to be developed.

## INTRODUCTION

Conventional impactors are useful for classifying particles as small as 1 μm diameter. Efforts to classify submicron particles have led to the operation of impactors at reduced pressures and, in some cases, very high jet velocities. Several applications make use of deposition of sonic and supersonic jets of fine particles on surfaces for formation of ultrafine particle films [1, 2] and for fine line pattern formation by aerosol jet etching (AJE) [3, 4]. The basic concept in AJE is the creation of a sonic or supersonic jet of ultrafine droplets of etchant with directional motion impinging on a masked substrate to be etched. In this manner, deep, fine lines may be etched, since the etching reaction proceeds immediately after a particle hits the substrate.

Present etching technology in microelectronics includes wet chemical etching and dry etching [5, 6]. Wet etching, in which wafers are immersed in aqueous etching solutions, is the oldest and when applicable, the least expensive process. Dry etching represented by plasma etching is performed in a low pressure gaseous plasma (neutral ionized gas). Aerosol jet etching is a technique that might have the potential for combining in a single method the high selectivity of wet etching process with a high degree of anisotropy of the dry etching method without some of the disadvantages of these methods. We present here our experimental investigation on the performance of the aerosol jet etching method. The experiments were carried out for three separate subjects in series: the formation and growth of submicron droplets, their low pressure impaction and finally their etching of the patterned substrates. Since the three experiments were connected in series, the conditions of a preceding experiment were readjusted to get better performance of the subsequent one if necessary.

## EXPERIMENTAL SYSTEMS AND PROCEDURES

A schematic diagram of the AJE system constructed for our experimental work is shown in Fig. 1. The first part of the apparatus is a spray system used for entraining etching solution in air as a carrier gas (1-20 *l*/min). We tried either pressure atomizer or ultrasonic humidifier. Etchant used in our experiment was mainly HF/water azeotropic mixture (38.2 wt% HF solution). The entrained etchant droplets pass through an evaporator where they vaporize. The evaporator with 30 mm ID and 210 mm length is heated outside with heating tape. The heat input is controlled by measuring the inside temperature of the evaporator mainly at 120℃ (the boiling point of the azeotrope) with a temperature controller in ± 0.1℃. The etchant vapor comes out of the evaporator through a hole at the inlet of a condenser and is met by cold sheath air (5-30 *l*/min) introduced to annular space around the hole. The condenser has 30 mm ID and variable length (300-900 mm). Homogeneous nucleation and subsequent growth of submicron droplets from the

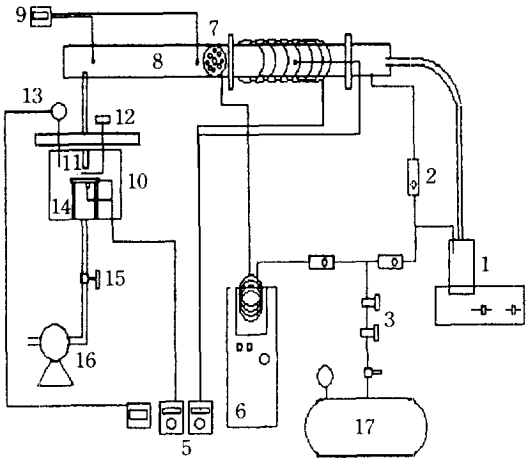


**Fig. 1. Schematic diagram of experimental apparatus.**

1. Ultrasonic humidifier 2. Flow meter
3. Air filter 4. Evaporator
5. Temperature controller 6. Cold bath
7. Sheath gas distributor 8. Condenser
9. Temperature indicator 10. Etching chamber
11. Nozzle 12. Shutter
13. Vacuum gauge
14. Substrate support (heater)
15. Valve 16. Vacuum pump
17. Air compressor

etchant vapor occur immediately after mixing of the vapor-laden carrier gas with the sheath gas. The sheath gas also plays a role of minimizing the vapor loss onto the condenser wall. The gas has been cooled in the cold bath maintained at $-10$℃ prior to meeting the vapor. Since we used air for both the carrier and the sheath gases and subsequent condensation of the vapor (including water) was greatly affected by the existence of moisture, the water content in the air was carefully controlled by the use of a freezing dryer.

This evaporation-condensation method has long been used for preparation of monodispersed submicron particles [7, 8]. The reason why we used the azeotrope as an etching solution is to minimize the effect of binary components on both the evaporation and the condensation.

Aerosol stream of the etchant from the condenser passes through 0.7 mm nozzle to an impaction chamber whose pressure is kept lower than atmospheric pressure (usually 50-100 Torr). The sonic stream impinges on a substrate and etches it. The temperature of the substrate is controlled by a temperature controller in $\pm 0.01$℃ and the pressure in the chamber is measured with a vacuum gauge in $\pm 0.01$ Torr. The

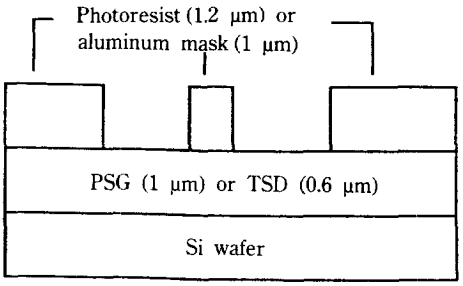


*PSG : phosphosilicate
TSD : thermal silicon oxide

**Fig. 2. Side view of etch samples.**

chamber pressure is controlled with a valve connected between the chamber and a vacuum pump. Chamber dimension is 200 mm ID×100 mm height. The substrate was protected from both pre- and post-etching by a shutter above it.

All the equipments were made of HF-resistant materials. Most of them were constructed of polymethylmethaacrylate (PMMA). The evaporator which operates at high temperature was made of stainless steel pipe internally coated with teflon particles in 1-mm thickness. To investigate formation and growth of submicron particles, only pure water was used in stead of the azeotrope since HF might harm a size measuring equipment. The particle size distribution was initially measured with electrical aerosol size analyzer (EAA, TSI 3030). Pressure atomizer was used for spraying the water. Process variables selected were the flow rates of carrier and sheath gases and the temperatures of carrier and sheath gases introduced at the condenser inlet. Based on some preliminary tests, patterned etching of silicon dioxide films with the HF azeotrope was finally conducted. Most of the samples used in this experiment were thermal oxide (TSD, 0.6 μm)-or phosphosilicate (PSG, about 10 wt% $P_2O_5$, 1 μm) films with dimensions of 1 cm×1 cm. The masks for etching on these samples were either of 1.2 μm-thick positive photoresist (AZ 1350J) or 1 μm-thick aluminum. Masks were patterned by lithography. The type of the etch sample is shown in Fig. 2. Surface morphologies were studied with ISI-DS-130 scanning electron microscope and etch depth was measured with Talystep. Process variables controlled for the main etching experiment were etch time, sheath gas flow rate and substrate temperature. The effects of these variables on etch performance such as etch rate, etched surface morphology, and anisotropy were investigated. The anisotropy is defined (Fig. 3) as $A_f = 1 - (w_m - w_r)/2d_r$, where $w_m$ is the width of the base of

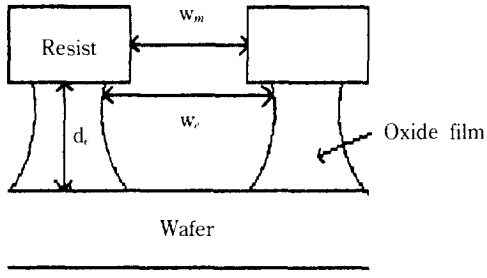


**Fig. 3. Crosssectional view of typical etched film.**

the mask line, $w_r$, the width of the top of the etched line, and $d_r$, the etch depth. In perfectly anisotropic (directional) etching, $A_f=1$, while $A_f=0$ in perfectly isotropic etching such as conventional wet etching.

## RESULTS AND DISCUSSION

### 1. Formation and Growth of the Submicron Droplets

The rate of liquid entrained through the pressure spray nozzle was increased from 0.2 to 2 ml/min linearly with the change in carrier gas flow rates from 5 to 20 *l*/min. Average size of the droplet as sprayed was 2-3 μm, depending on the flow rate of carrier gas. The temperature at the condenser inlet depends on the temperature of evaporator, the ratio of carrier to sheath gas flow rates and the temperature of sheath gas. The mixing pattern of the carrier and sheath gases around the hole is expected essential in formation and subsequent growth of submicron droplets. However, EAA data did not directly indicate size evolution of the ultrafine droplets in the condenser due to their evaporation in the EAA. Therefore it was believed that the data from the EAA only revealed approximate results. Table 1 shows some of the values on total droplet number concentration which were the most reliable among the EAA data. Average diameters of the droplets were estimated from these total number concentrations and the amount of the liquid sprayed, and they are also shown in the table. To confirm the average size of the droplets, the equation of droplet evaporation was set up including noncontinuum and Kelvin effects [7], and integrated during the time equal to residence time of the droplets in EAA. As a result the size of the droplets at the exit of the condenser was estimated to be about 0.1 to 0.3 μm which is comparable to the sizes in the table.

As shown in the table, total droplet number concentrations increases with the carrier gas flow rate. It is due to higher water content in the carrier gas as described earlier. The fact that the average droplet size is insensitive to the variation of the carrier gas flow rate implies the typical phenomena of coupled nucleation and condensation processes. Increased water content resulted in higher supersaturation and this causes higher rates of both nucleation and condensation. The former gives formation of smaller nuclei but the latter gives their faster growth. Therefore, the droplet size seems almost independent of the carrier gas flow rate.

As the flow rate of the sheath gas is raised with that of the carrier gas fixed, both the total number concentration and the average diameter of the droplets decrease. Due to dilution effect of the sheath gas, the decrease in the number is obvious. The decrease in the size is explained by the fact that more sheath gas cools the vapor more rapidly at the point of encounter between two gases, before dilution is about to happen. This increases the saturation ratio and produces smaller nuclei.

Higher temperature of the evaporator makes less droplets with increased diameter due to the decrease in saturation ratio, as shown in the table.

### 2. Impaction and Preliminary Etching

Linear velocity of the jet through nozzle was calculated based on the measurement of volumetric flow rate through the etching chamber. The velocity increased as chamber pressure decreased from atmospheric pressure to about 400 Torr which is the 'critical pressure' for the jet to be sonic. Below 400 Torr the jet velocity kept constant at 230 m/s and 260 m/s with 0.7 mm- and 0.35 mm-diameter nozzles, respectively. The air properties at the nozzle upstream were used in this calculation. The efficiency with which particles of diameter $d_p$ and mass density $\rho_p$ in a vertical jet impinges on substrate is dependent on several parameters: the ratio of the nozzle-to-substrate distance to the nozzle inside diameter (S/D); the Reynolds number of the jet; impactor body geometry; Stoke's number $\varphi$, $\varphi=\rho_p U_j d_p^2 C/18\ \mu D$, where $U_j$ is the exit jet velocity, D the exit jet diameter, μ the viscosity of the gas in the jet, and C the Cunningham correction factor which considers the noncontinuum effect on particle drag. The diameter of a particle which is collected with a 50% efficiency is referred to as the 'cutoff' diameter and the corresponding Stokes number is referred as the $\varphi_{50}$. Jurcik et al. [8] and Flagen [9] reported that the flow from an underexpanded sonic jet expands to supersonic velocities before decelerating through a shock wave between the jet outlet and the impaction plate. Biswas and Flagen [10] showed that the 50% cutoff Stokes number, $\varphi_{50}$, does not ap-

**Table 1. Total number concentration and estimated average size of the droplets**

| Carrier gas flow rate(*l*/min) | Sheath gas flow rate(*l*/min) | Evaporator temperature(℃) | Total number concentration(droplets/cc) | Average diameter(μm) |
|---|---|---|---|---|
| 17.5 | 15 | 100 | $2.70\times10^{9}$ | 0.26 |
| 12.5 | 15 | 100 | $1.66\times10^{9}$ | 0.26 |
| 7.5 | 15 | 100 | $3.66\times10^{8}$ | 0.25 |
| 12.5 | 30 | 100 | $1.13\times10^{9}$ | 0.20 |
| 12.5 | 15 | 125 | $9.79\times10^{8}$ | 0.31 |

pear to vary significantly with the jet pressure ratio, Mach number, or the particle Knudsen number when $\varphi$ was computed in terms of the fluid properties at stagnation point on the impaction plate. They indicated that the value of $\varphi_{50}$ was $0.09\pm0.1$. Though it is uncertain that the value of S/D in our impactor (S=9 mm, D=0.7 mm, and S/D=13) is within the range of S/D of their impactor, $d_{50}$ was estimated based on their $\varphi_{50}$ value. The diameters were found to be 0.1628, 0.1118 and 0.0404 μm when the pressure recovery at stagnation point on the plate were assumed 50, 30 and 10%, respectively. Pressure recovery here is defined as the ratio of the stagnation pressure on the impaction plate to the nozzle upstream pressure. Since we did not measure the stagnation pressure, exact $d_{50}$ could not be reported. According to Biswas and Flagen, pressure recovery drops to far less than 50% at the ratio of nozzle upstream to chamber pressures of 0.11 which was maintained in our experiment. The value of $d_{50}$ might be, therefore, about 0.05 μm. It was concluded that since the particles we produced has average diameters of 0.1 to 0.3 μm, they could be collected on the substrate in the chamber.

Some preliminary tests were carried out prior to the experiment on patterned etching. One of them was etching of slide glass with HF/water azeotrope. Fig. 4 shows a typical morphology of HF-etched glass surface pictured with scanning electron microscope. Fig. 4(a) is as-etched surface before ultrasonic washing with acetone and water. There appear solid residues on it, which were also seen as white residues with the naked eyes. They are estimated to be $H_2SiF_6$ (white powder) from the reaction:

$$SiO_2 + 6HF = H_2SiF_6 + 2H_2O$$

Washing removes the layers of the solid residues as shown in Fig. 4(b). Small holes in multilayer are observed, which must be created by the impingement of the etchant droplets. The average size of the holes is comparable to that of the droplets observed earlier by other means.

For patterned etching, the experimental conditions were readjusted as in Table 2 in order to improve

a. without washing

b. with washing

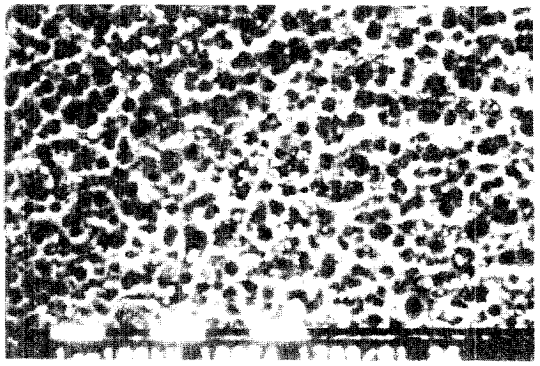

**Fig. 4. Etched surfaces of slide glass.**
Etching conditions: nozzle diameter=0.7 mm, carrier gas flow rate=1 *l*/min, sheath gas flow rate=8 *l*/min, etching chamber pressure=90 torr, etch time=3 min, substrate temperature=50℃.

performance of the process. As described earlier, the temperature of condenser, in particular, at the point of mixing of the vapor-laden carrier gas with the cold sheath gas, is very important. The temperatures at the point were measured to be 80, 67 and 57℃, depending on the sheath gas flow rates of 5, 8 and 11 *l*/min, respectively. The temperature of the condenser exit, however, remains constant ($27\pm2$℃) irrespective of the conditions at the mixing point.

**Table 2. Experimental conditions for patterned etching**

| Process variables | Values |
|---|---|
| Spray system used | Ultrasonic humidifier |
| Spray rate of etchant | 0.6 ml/min (fixed) |
| Carrier gas flow rate | 1 *l*/min (fixed) |
| Evaporator temperature | 120℃ (fixed) |
| Sheath gas flow rate | 5, 8, 11, 20 *l*/min |
| Sheath gas temperature | −10℃ (fixed) |
| Nozzle diameter | 0.7 mm |
| Chamber pressure | 90 Torr |
| Substrate temperature | 25, 50, 75, 100℃ |

## 3. Patterned Etching

Based on the results of the previous separate experiments, patterned etching of $SiO_2$ (PSG or TSD) films with aluminum or photoresist mask were conducted. With some preliminary tests, PSG films were preferentially used since the etch rate of TSD films were too slow to get appreciable etch depth. As for masks aluminum masks were rarely used due to their difficulty of cleaning compared to the corresponding photoresist masks.

Fig. 5 has scanning electron micrographs, which show the morphologies of the bottoms [(a), (b)] and the side wall (c). The bottom surface in Fig. 5(a) has mid-etched $SiO_2$ film, whose surface looks similar to Fig. 4. In Fig. 5(b), where etching has been completed to the bottom of PSG film, Si water surface underneath has been exposed. Scratches were always observed on the side wall as in Fig. 5(c), which might be the characteristics of the AJE and should be investigated further in relation with droplet movement near and on the substrate surface.

Etch depth vs. time was plotted in Fig. 6 for the different temperatures of substrate. For all the curves in the figure, etch rate is initially high and then slightly slows down due to the formation of either the residues or the multilayer of the etchant on the surface. Among them the curve of 100℃ reveals an initial induction period necessary for surface cooling to steady-state temperature before there appears the usual trend as other curves. During the period, since some droplets evaporate, approaching to the substrate, etch does not occur appreciably until the surface cools down.

The effect of substrate temperature on the etch depth appears on Fig. 7 for the different values of sheath gas flow rate. As shown in the figure, the maximum etch rate occurs at 50℃. It is explained that evaporation rate of the droplets on or above the substrate surface seems to dominate that of the surface reaction at temperatures above 50℃. The decrease in etch rate

a. bottom surface-before breakthrough (with aluminum mask)

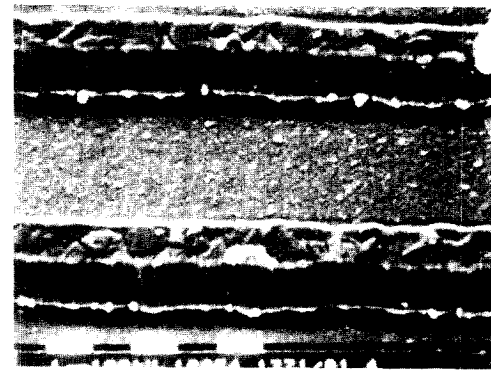

b. bottom surface-after breakthrough (with aluminum mask)

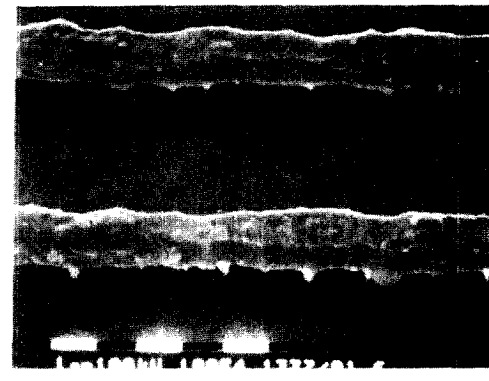

c. side wall (with photoresist)

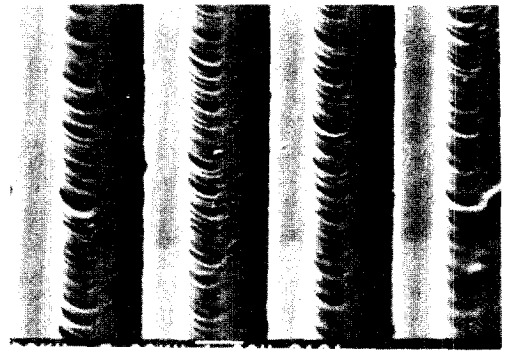

**Fig. 5. Etched surface morphology for AJE of PSG films.**

was well realized on the SEM images.

Fig. 8 shows the effect of sheath gas flow rate on the etch depth. Higher sheath gas flow rate reduces the etch depth due to the decrease in number concentration and size of the droplets as noted earlier. The variation is less significant with increase in substrate

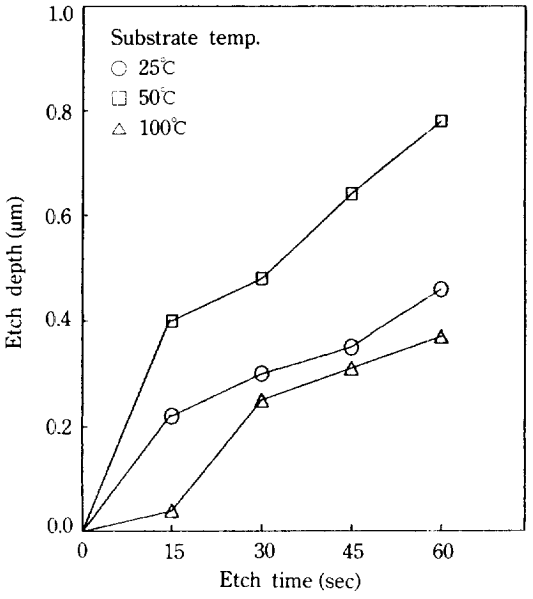


**Fig. 6. Etch depth vs. time.**
Etching conditions: nozzle diameter=7.0 mm, carrier gas flow rate=1 *l*/min, sheath gas flow rate=8 *l*/min, etching chamber pressure=90 torr.

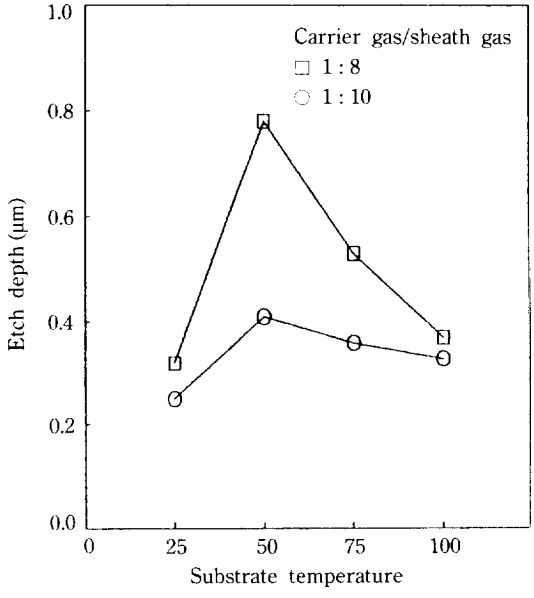


**Fig. 7. Effect of substrate temperature on etch depth.**
Etching conditions: nozzle diameter=0.7 mm, etching chamber pressure=90 torr, etch time=1 min.

temperature since evaporation also reduces both the number concentration and the size. The sheath gas effect is supported by the SEM images of Fig. 9. Fig. 9

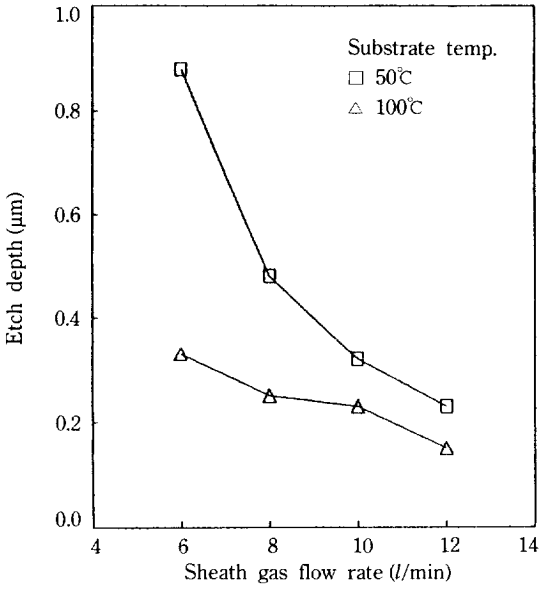


**Fig. 8. Effect of flow ratio on etch depth.**
Etching conditions: nozzle diameter=0.7 mm, carrier gas flow rate=1 *l*/min, etching chamber pressure=90 torr, etch time=30 sec.

**Table 3. Measured anisotropies for various conditions**
Etching conditions: nozzle diameter=0.35 mm, carrier gas flow rate=1 *l*/min, etching chamber pressure=90 torr, etch time=3 min

| Substrate temperature(℃) $T_s$ | Sheate gas flow rate / Carrier gas flow rate | Anisotropy, $A_r$ |
|---|---|---|
| 25 | 8 | 0.50 |
| 50 | 8 | 0.53* |
| 75 | 8 | 0.56 |
| 100 | 8 | 0.58 |
| 50 | 5 | 0.42 |
| 50 | 11 | 0.63 |

*calculated at etch time=1 min 30 sec

(a) was obtained at reduced sheath gas flow rate (the flow ratio of sheath to carrier gas=5) under which more (number) and larger (size) droplets were produced. The feature of the surface is similar to that of an uncontrolled wet-etched surface. As both the number concentration and the size of the droplets decreases at the flow ratio of 11, the etching performance is significantly improved as shown in (b).

Anisotropy was measured also from the SEM pictures. The measured anisotropies range from 0.4 to 0.65 shown in Table 3. The highest anisotropy was obtained when both the substrate temperature and the sheath gas flow rate were high. This tendency is coincided

a. sheath gas flow rate=5 *l*/min

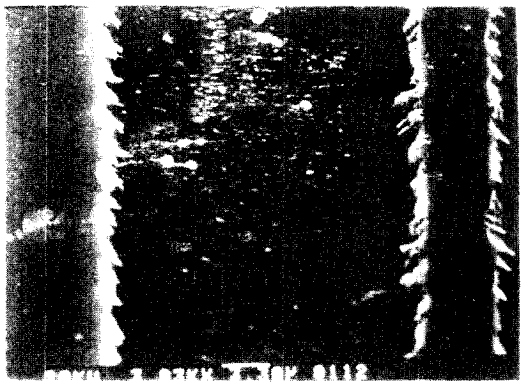

b. sheath gas flow rate=11 *l*/min

**Fig. 9. Scanning eletron micrographs for AJE of PSG films at various flow ratios.**
Etching conditions: nozzle diameter=0.7 mm, carrier gas flow rate=1 *l*/min, etching chamber pressure=90 torr, etch time=3 min, substrate temperature=50C.

with the direction of lowering the etch rate and raising the controllability of the etching.

## CONCLUSION

In summary, aerosol jet etching (AJE) differs from the conventional wet etching in using the submicron droplets of etchant in order to increase the efficiency of the etching and the controllability of the etch rate. The former, the efficiency includes both the reduction in mass transfer resistance around the surface and the economic use of the etchant without production of excess waste which might cause the environmental problem. The latter, the controllability consists of the performance and the directionality of etching. The trend of decreasing the etch rate coincides with that of increasing the controllability and the directionality of etching.

To get better performance with AJE, the particle size should be further reduced and the corresponding chamber pressure should be also lowered so as to guarantee the deposition of the smaller particles. Some other techniques to suppress the formation of the multilayer need to be developed in order to maximize the advantages of AJE and to compete with the prevailing dry etching methods.

## REFERENCES

1. Kashu, S., Fuchita, E., Manabe, T. and Hayashi, C.: *Jpn. J. Appl. Phys.*, **23**, L910 (1984).
2. Fukuysma, K., Yamada, I. and Takagi, T.: *J. Appl. Phys.*, **58**, 4146 (1985).
3. Chen, Y. L., Brock, J. R. and Trachtenberg, I.: *J. Appl. Phys. Lett.*, **51**, 2203 (1987).
4. Chen, Y. L., Brock, J. R. and Trachtenberg, I.: *Aerosol Sci. Technol.*, **12**, 842 (1990).
5. Ruska, W. C.: Microelectronic Processing, McGraw-Hill, New York (1988).
6. Runyan, W. R.: Semiconductor Integrated Circuit Processing Technology, Addison-Wesley, New York (1990).
7. Fuchs, N. A.: The Mechanics of Aerosols, Pergamon, Oxford (1964).
8. Hinds, W. C.: Aerosol Technology, John-Wiley & Sons, New York (1982).
9. Chon, B.: M. S. Thesis, Chung Ang University (1991).
10. Jurcik, B. J. Jr., Brock, J. R. and Trachtenberg, I.: *J. Aerosol Sci.*, **20**, 701 (1989).
11. Flagen, R. C.: *J. Colloid Interface Sci.*, **87**, 291 (1981).
12. Biswas, P. and Flagen, R. C.: *Envir. Sci. Technol.*, **18**, 611 (1984).